R&D on X-Band Accelerating Structures at the INFN-LNF

D. Alesini, R. Boni, A. Gallo, F. Marcellini, B. Spataro
INFN-LNF, Via E. Fermi 40 00044 Frascati (Roma), Italy;

L. Ficcadenti, M. Migliorati, A. Mostacci, L. Palumbo
Univ. of Rome I, "La Sapienza", Dip. Energetica, Via A. Scarpa 14, 00161, Roma, Italy

A. Bacci
INFN Via Celoria 16 20133 Milano, Italy

ABSTRACT

The development of ever more advanced accelerating structures is one of the leading activity of the accelerator community. High accelerating gradient, efficiency, reliability of the accelerating structures have strong and positive impact on linear accelerator projects. The availability of reliable microwave power sources and components from the industry, have made possible to develop RF structures operating at very high frequencies with higher accelerating gradient.

This report describes the studies and the activities carried out by LNF, in collaboration with other national Institutions, for the development of high performance X-band accelerating structures.

1 INTRODUCTION

To upgrade the perfomances of the Linacs and particularly to keep their length within reasonable limits, the accelerator community have concentrated resources and efforts to study and develope ever more performing accelerating structures. The main goal is to achieve higher accelerating gradients and reliability.

The superconducting cavities have reached performances that were unthinkable just a few years ago. New manufacturing tecniques and sophisticated cleaning processes permitted to achieve, almost routinely, L-band RF gradients well above 30 MV/m with some excellent results close to 40 MV/m.

The room-temperature accelerating structures too are being subject of intense R&D, to reach higher gradient and reliability. In alternative to the widely diffused S-band sections, C-band and X-band structures have been considered since their reduced size and the high operating frequency which allows to reach higher gradients.

The LNF, in collaboration with University of Roma-1, decided to dedicate resources and man-power to study and develope advanced X-band accelerating structures to be used in the INFN SASE-FEL linac projects [1]. In particular, the motivation of this activity was to compare travelling wave (TW) and standing wave (SW) X-band device features and to optimize a reference model by taking in consideration different operating modes. The first and most urgent application will be the construction of an X-band device for the SPARC beam longitudinal emittance compensation [2]. Also, the LNF research activity aims to gain experience in manufacturing and brazing processes of X-band RF structures.

2 PROPOSED X-BAND STRUCTURE FOR THE FRASCATI PHOTO-INJECTOR LINAC PROJECTS

The multi-cell RF structures, which find application in linear accelerators, can be divided in two groups: the Standing-Wave and the Traveling-Wave ones. The detailed analysis of the SW and TW structures is not the purpose of this report and can be found in [3, 4]. However it can be said that both types of structures have advantages and drawbacks according to their use in linear accelerators.

In general, the TW sections are preferred when rather long straight lines are available for acceleration and when several units are needed to reach the final accelerator energy. In fact, the TW sections are basically input matched and expensive devices like circulators or isolators are not necessary to protect the RF source because the power, not dissipated through the section, after traveling along it, is absorbed by an external load. Furthermore, because of their low sensitivity to the temperature and to manufacturing imperfections they can be produced in long units, thus getting better the linac filling factor.

The SW structures instead, have one coupling port and the e.m. fields build-up through multiple reflections. They are better-suited when special actions or manipulations of the beam are required or when high field gradient are necessary in a short beam line length. Also, too long SW structures are not recommended because of the needed tight mechanical tolerances and the risk of overlapping of neighbouring modes.

The SW structures have another advantage that can be very important in high gradients operation. The SW units do not withstand internal discharges without being strongly detuned. This results in less breakdown damage of the inner surfaces since the generator cannot power the structure, that is suddenly mismatched. On the contrary, the TW structures, being connected to an external load, can hold up an internal discharge so they may be seriously damaged. In addition, the SW units will likely have lower breakdown rate due to their reduced surface peak fields [5].

For each type of accelerating structure, the mode of operation must be carefully analyzed to select the most suitable model to our purposes. Some basic features of SW and TW structures are briefly compared in table 1. They are generally common to all the structures, whatever is the frequency band, although the table refers mainly to X-band devices.

Table 1: Basic features of linear accelerating structures.

	SW	**TW**
Average accelerating field	High	Low
Filling time	Proportional to the quality factor: generally longer than TW (~0.5µs @ 11.424 GHz)	Proportional to group velocity and length: shorter than SW (~0.1 µs @ L=1m)
Total length (L)	The cell number (for a π-mode) is limited to about 10-15 because of mode overlapping. Thus, L $\cong$ 10-20cm	The maximum length should be [1÷2]/α (with α = attenuation constant $\cong$ 0.6m^{-1} @ 11.4 GHz). L $\cong$ 1-2m at 11.4 GHz
Total accelerating voltage vs. L	$V \propto L^{1/2}$	$V \propto (1-e^{-\alpha L})/\alpha$
Power system considerations	Circulator needed to protect the klystron	Circulator not necessary.
Maximum surface electric field.	Better high gradient performances	Worse high gradient performances
Temperature sensitivity	High	Lower than SW's.
Wake fields intensity	Low	High

2.1 SW accelerating sections: π and π/2 modes X-band structures.

The modes π and π/2 of the SW structures have been analyzed and their characteristics have been compared. The longitudinal electric field Ez snapshots of π and π/2 modes of SW devices are schematically depicted in Fig. 1. According to the Brillouin diagram of a disk loaded waveguide (Fig. 2), the π/2 resonance lays on a high slope position of the pass-band curve while the π mode one lays on a zero slope point. Thus, the π mode can be very close to neighbouring modes if the structure is made of many cavities. Therefore, it requires fine mechanical construction and tuning to get frequency stability and precise mode configuration to avoid mode overlapping. The π/2 mode units are less sensitive from this point of view but, on the other hand, are less efficient because half the cavities does not contribute to the accelerating field. Their manufacturing is somewhat complicate too.
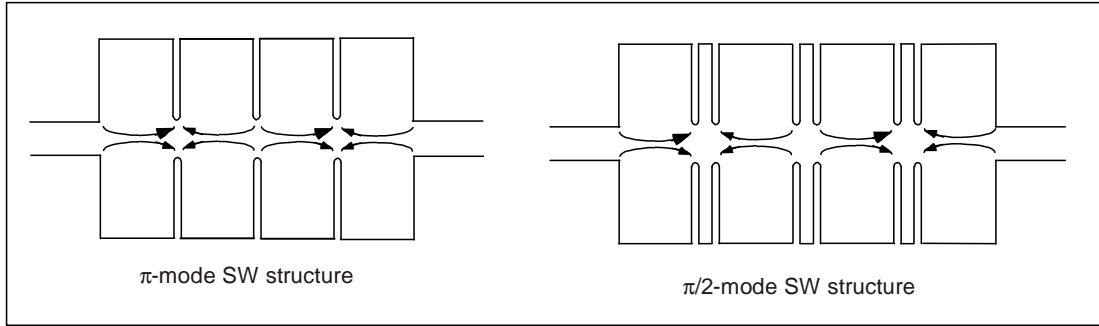
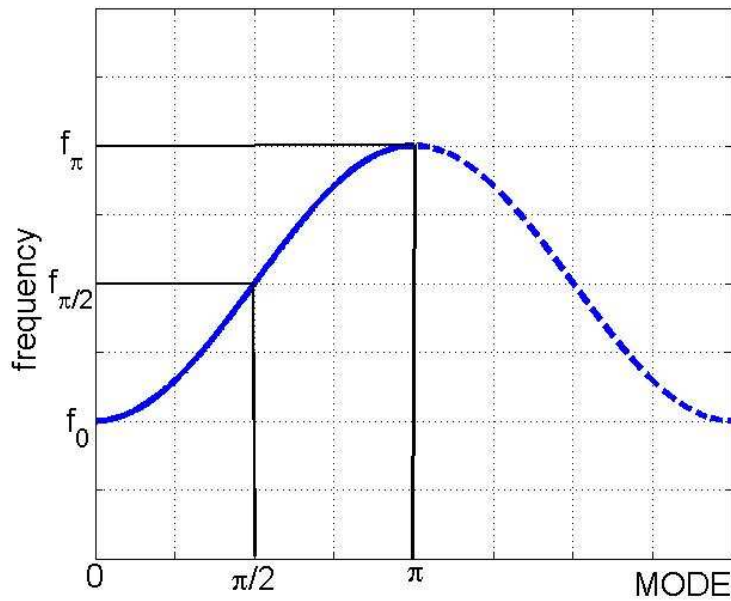Figure 1: Longitudinal electric field in π and $\pi/2$ SW structures.

Figure 2: Brillouin diagram of a multi-cell cavity.

Two X-band prototypes have been realized. The first one is a 9 cells π-mode section with central input coupler to avoid excitation of the adjacent $(8/9)\pi$ mode. The design details of the X-band π mode SW structure can be found in [6]. The Fig. 3, shows the copper prototype (left), ready for bench test and the brazed model (right). The input tapered waveguide is coupled to the mid-cell with a slot, opened on the outer wall in order to obtain a coupling coefficient (β) equal to 1. The electromagnetic design of the structure has been carried out with the computer codes [14] including a full thermal analysis characterization [15]. Details of the structure shape are shown in Fig. 4 and its main parameters are listed in Table 2 (data in Italics refer to a possible application to SPARC). The Fig. 5 shows the electric field profile on axis of the π-mode, measured with the bead perturbation method. The field flatness has been obtained by slightly reducing the end-cells radius and by tuning each cells with small cylinders.

The second structure prototype is the $\pi/2$ SW cavity shown in the figures 6, 7, and 8. Measurements on the prototype are in progress.

5

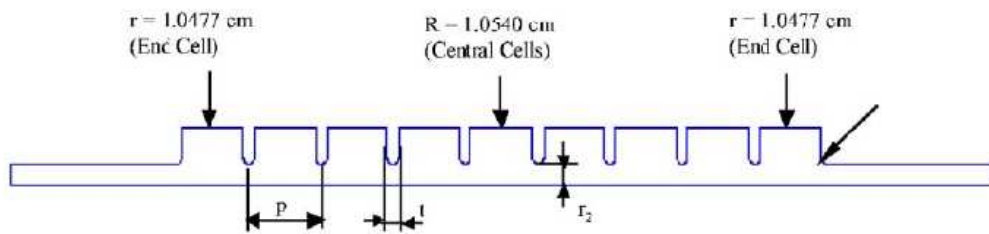Figure 3: prototype and brazed copper model of the X-band π-mode SW structure under development at LNF

Figure 4: Shape of the 9-cell SW, π-mode X-band section.

Table 2: Main parameters of the X-band π-mode structure

Frequency (GHz)	11.424
Cells length (mm)	13.12
Number of cells	9
Beam holes radius (mm)	4
Iris thickness (mm)	2
Transit time factor	0.731
Quality factor Q	8400
R/Q (Ω/m)	9165
Coupling coefficient K	2.42
Peak input power (MW)	*2.7*
Duty cycle	10^{-4}
Repetion rate (Hz)	*50*
Average dissipated power (W)	*270*
Peak axial electric field (MV/m)	*57.5*
Kilpatrick factor	*1.197*
Peak surface electric field (MV/m)	*105*
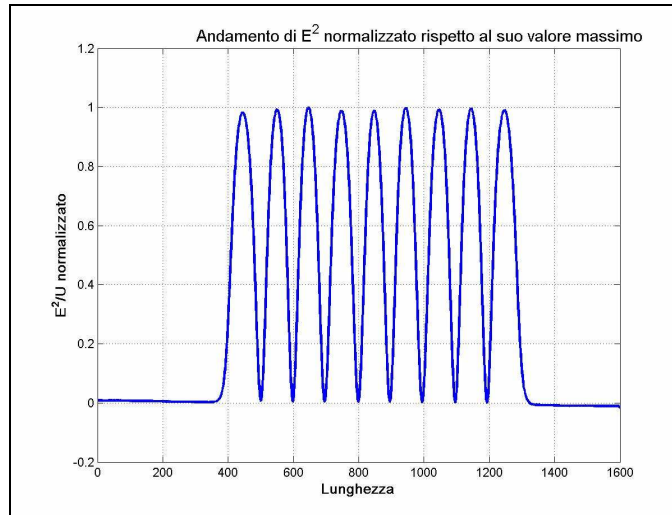
Figure 5: Measured E field profile for the π mode copper model.
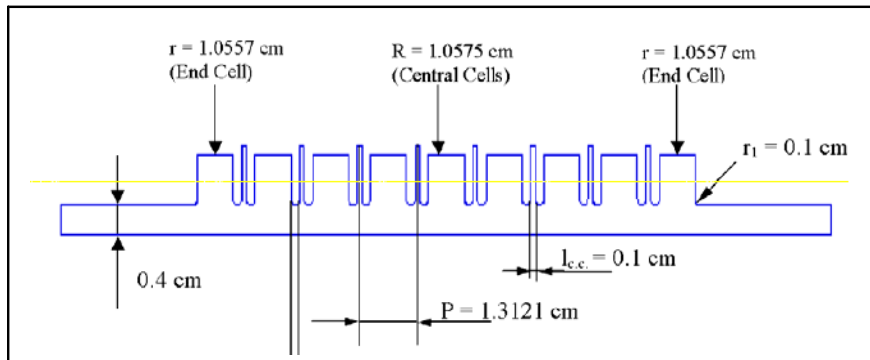
Figure 6: Shape of the 9-cell SW, $\pi/2$-mode X-band section
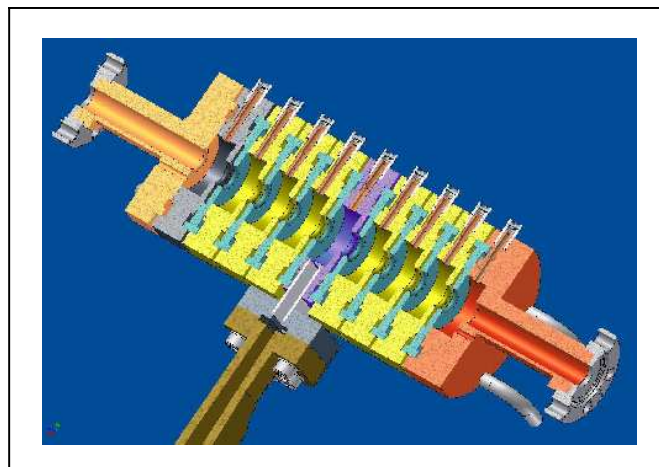

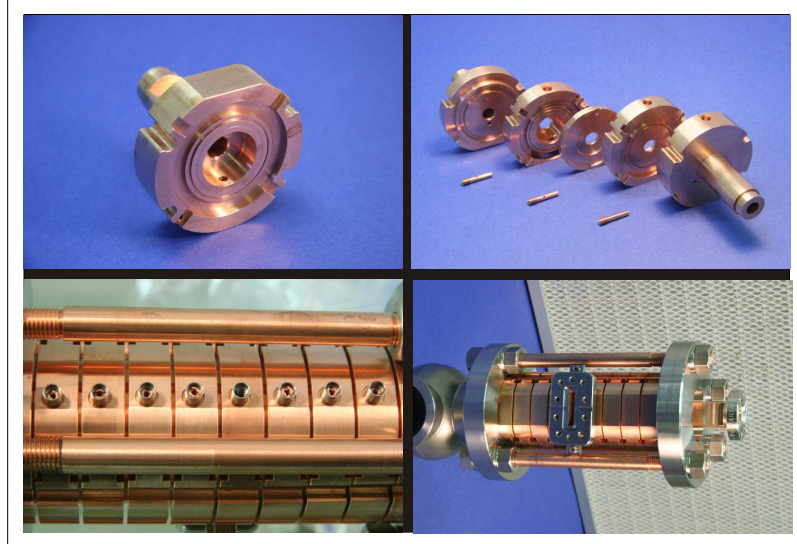*Figure 7: $\pi/2$ cavity 3D mechanical drawing.*

Figure 8: Fabrication details of the $\pi/2$ copper prototype.

2.2 TW accelerating sections: the (5/6)π model

We have studied extensively the standing wave structures, as they are more pertinent to the INFN present projects. Nevertheless, we have studied the electromagnetic properties of (2/3)π and (5/6)π travelling wave structure in the light of possible applications in future activities.

Since the 60's, with the construction of the 2-mile accelerator at Stanford, the most utilized TW structure in linear accelerators has been the (2/3)π one because of its highest shunt-impedance per unit length. High shunt impedance implies better efficiency that means low RF power wasted per unit length and, in practice, less wall-plug power and shorter accelerators. However, recent experiences made by the SLAC-KEK NLC group [7], evidenced that the (5/6)π structures are less discharge-prone than the (2/3)π ones, in the very high gradient regime. Also, the (5/6)π, with its higher phase-advance per cell, i.e. the larger cell iris, meets the short range wake-field requirements much better than the (2/3)π [8]. Table 3 compares some important parameters of a (2/3)π and (5/6)π TW structures. Figure 9 shows the field profile and the phase-advance per cell of a 7-cell (5/6)π linear structure obtained by HFSS.
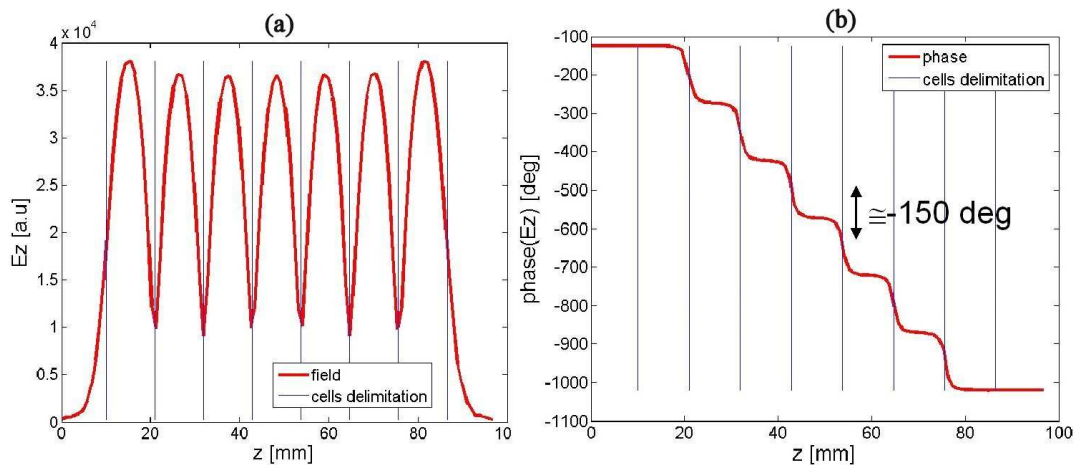

Figure 9: Magnitude (a) and phase (b) of the electric field of a 7 cells (5/6)π TW structure.

Table 3 - (2/3) π and (5/6) π structures parameters

MODE	Parameters					
	Group velocity (v_g/c [%])	Quality factor per unit length (Q)	Shunt impedance per unit length ($r=E^2/p_{diss}$ [MΩ/m])	Shunt resistance per unit length ($z=E^2/P$ [MΩ/m])	r/Q ([kΩ/m])	Attenuation (α [1/m])
(2/3) π	3.23	6653	86.92	96.73	13.1	0.57
(5/6) π	1.92	7855	90.43	143.6	11.5	0.79

3   RF POWER COUPLING SYSTEM

The RF power is coupled to the accelerator structure by means of apertures (or slots) applied to the cylindrical wall of a cavity cell. The magnetic field of the waveguide TE$_{01}$ propagating mode couples the circular flux lines of the input cavity magnetic field. The slot area is determined with 3D computer codes and is set to match the load (the accelerating structure in this case) to the RF source. Before the extensive use of computer codes, the slot area was determined with an iterative "cut and try" procedure on prototypes models. A smooth tapering of the input waveguide usually helps in achieving a good matching.

Figure 10 shows the input coupler design drawing of the π-mode SW X-band structure and the tapered waveguide. The dimension of the coupler window (w) and of the central cell radius (R$_c$) have been tuned in order to obtain simultaneously a coupling coefficient $\beta = 1$, a resonant frequency of the whole system (cells+coupler) equal to 11.424 GHz and to preserve a good field flatness. Figure 11 shows the magnitude of the reflection coefficient at the coupler input port, obtained by HFSS, after the optimization of the coupler dimension. In the same figure it is reported the normalized electric field on axis at the π-mode resonant frequency. The input matching obtained at the nominal frequency 11.424 GHz corresponds to the standing ratio SWR < 1.1.
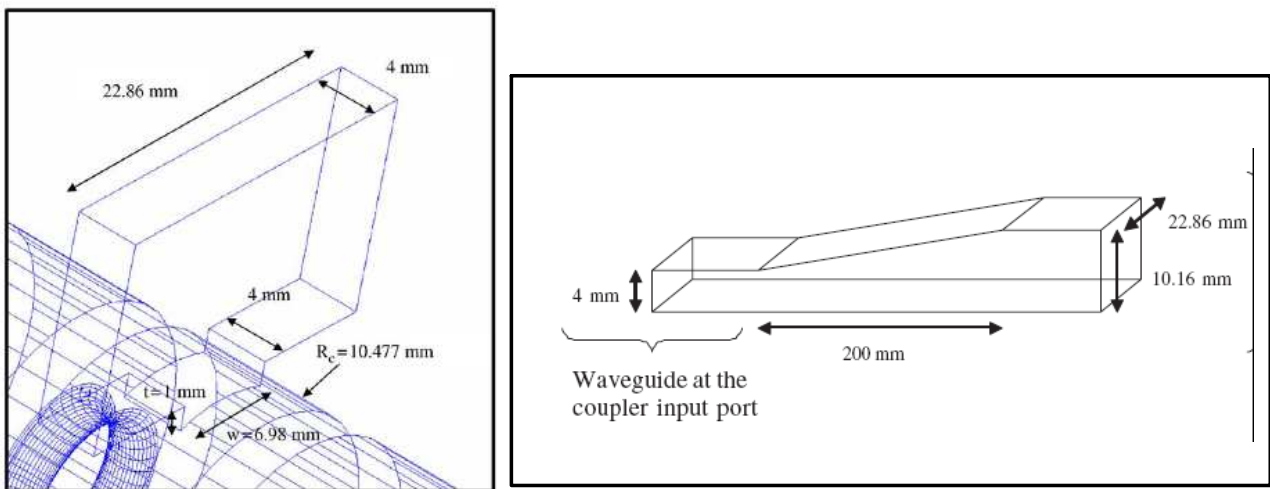

Figure 10: input coupler of the π-mode SW 11.424 GHz structure
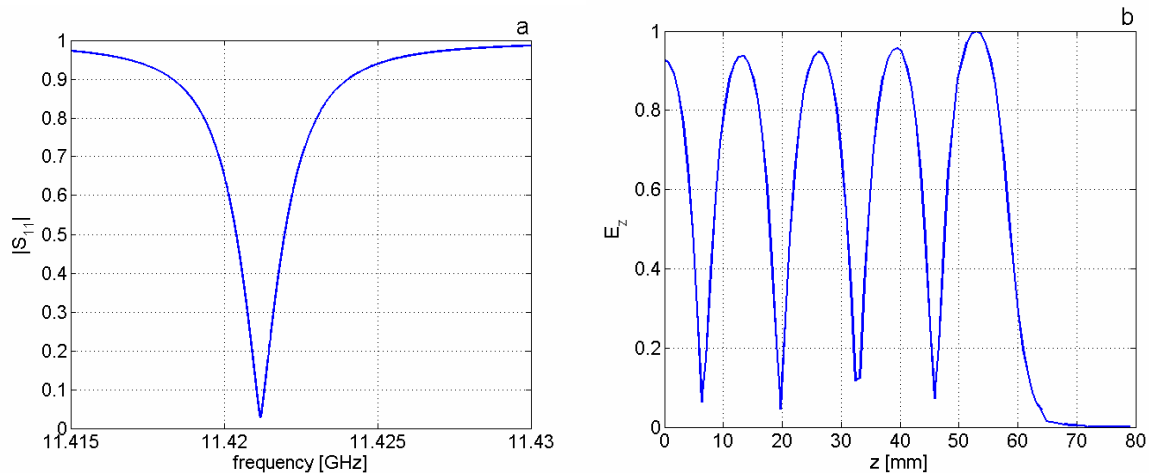
Figure 11: Simulated reflection coefficient at the coupler port and normalized electric field on axis at the π -mode resonant frequency (HFSS simulations).

In Fig. 12, the dimensions of the coupler window and cell related to the $5/6\pi$ traveling wave structure are reported. In this case the coupler sizes have been optimized in order to get a perfect matching between the feeding waveguide mode and the traveling section. The simulations results give a reflection coefficient less than 0.01.
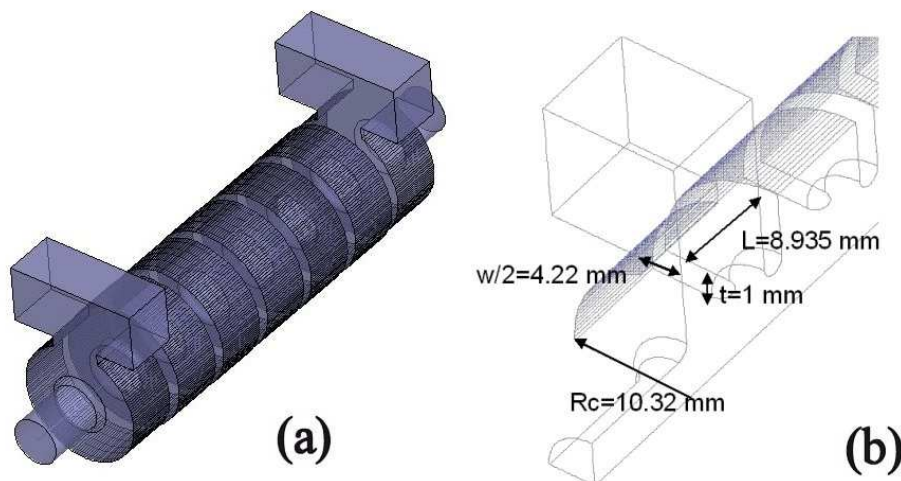

Figure 12: HFSS model of the $5/6\pi$ traveling wave structure (a) and coupler dimensions (b).

3.1 Coupler asymmetry effects

The RF coupler matching slots of TW and SW structures break the symmetry of the accelerating structure input cavity cell and provide a slight deformation of the electric and magnetic field lines (Fig. 13). A non zero transverse component of the magnetic field on axis can give to the beam a transverse kick that can negatively affect the beam quality. The problem was initially pointed out [9,10] at SLAC, on the S-band 2-mile TW LINAC sections and the solution adopted was to move the position of the coupling cavity iris closer to the matching slot to compensate for the magnetic deflection with an electric one (Fig. 14): the required shift Δx is some 2 millimeters in S-band structures. We have studied the compensation tecnique for the $(5/6)\pi$ mode X-band TW structure under development at LNF using the HFSS code. Fig 15 shows the transverse magnetic and the transverse

electric field components after the off-setting of the iris. To have a complete compensation a Δx =0.45 mm is required.
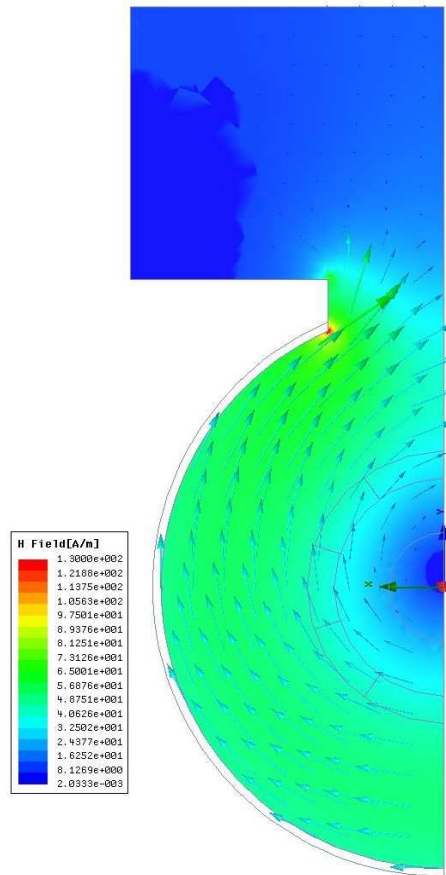

Figure 13: distorsion of the magnetic field lines due to the presence of the coupler window.
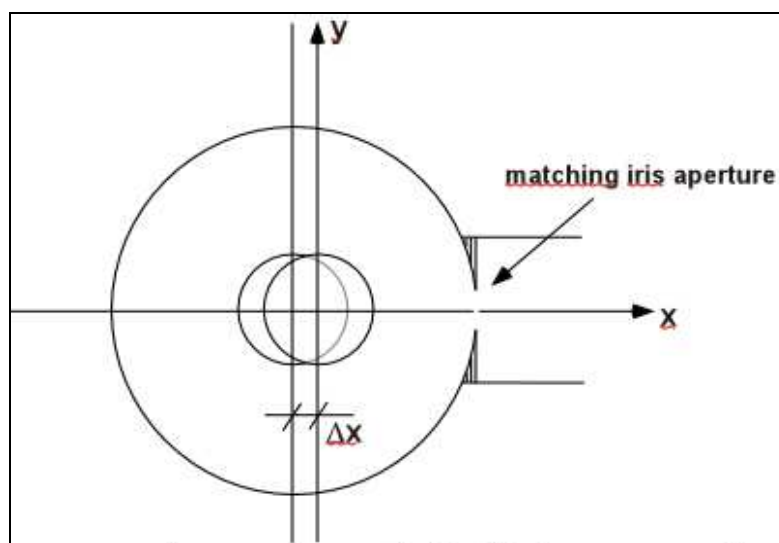

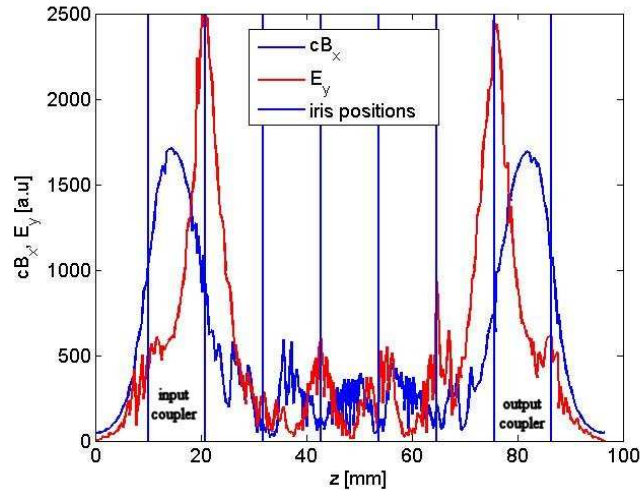*Figure 14: coupler offset to compensate the magnetic kick due to the coupler asymmetry.*

11

Figure 15: Transverse magnetic field on axis and compensation with electric field for the (5/6)π X-band TW structure (HFSS results).

An alternative compensation technique (Fig. 16) consists in feeding the same amount of power through two identical coupling slots located on the opposite sides of the input RF coupling cell [11]. A well balanced magic tee is necessary to split the RF power in equal amounts and with opposite phases. The case of a symmetric coupler has been studied with HFSS for the (5/6)π X-band TW structure. The 3D model and the final dimensions are shown in Fig. 17.

Another elegant solution to the symmetric coupling for an S-band structure can be found in [12]. It consists of a J-shaped single waveguide feeder which supplies the input cavity from two opposite counter-phase coupling slots. The counter-phase tuning is made by changing the guide wavelength with the adjustment of the input waveguide width. The signal delay between the slots is negligible for the usual applications in linear accelerators. The same application to a C-band structure [13] is shown in Fig 18. We are aiming to study the application of this solution to the X-band 5/6π accelerator structure.
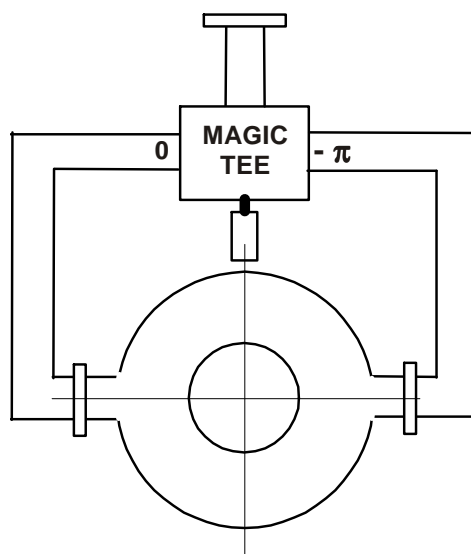

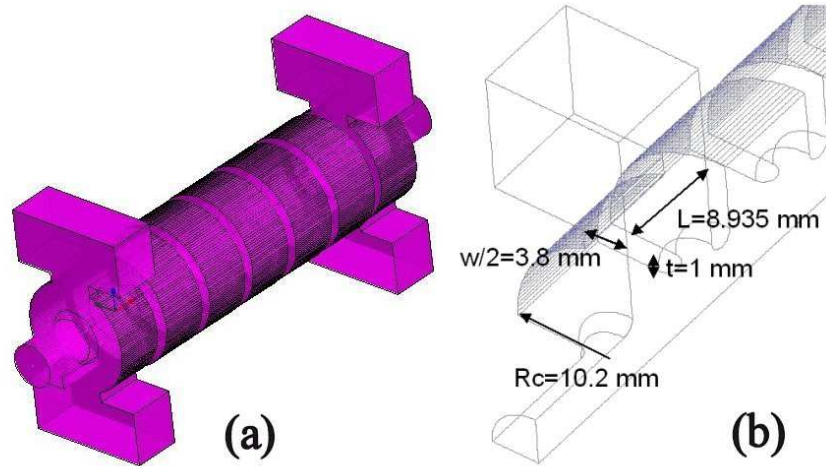*Figure 16: the symmetrical double side coupling.*

12

Figure 17: HFSS model of the 5/6π traveling wave structure with symmetric coupler (a) and coupler dimensions (b).
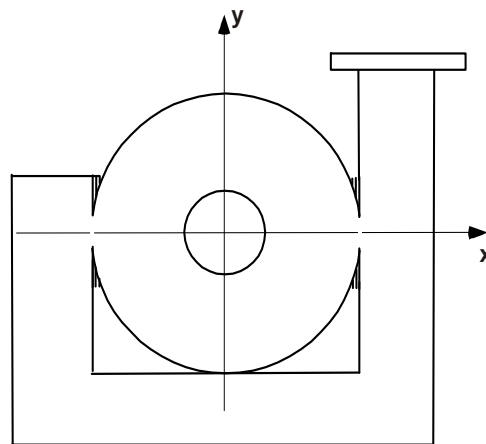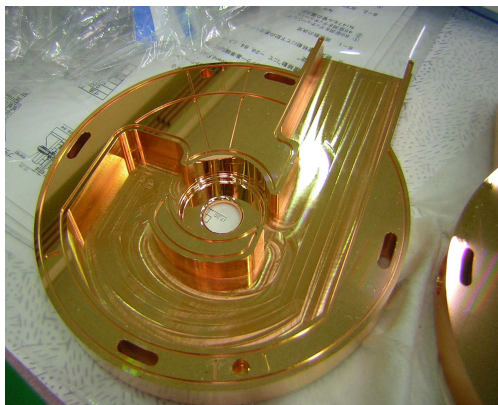

Figure 18: C-band symmetric coupling (photo courtesy of Mitsubishi Heavy Ind., Mihara, Japan)

5   ACKNOLEDGEMENTS

References

1)   L. Palumbo et al., "The SPARC Project: A High Brightness Electron Beam Source at LNF to Drive a SASE-FEL Experiment ", Proceedings of the PAC2003, Portland, May 2003, p. 3285.
2)   D. Alesini et al., "Design and RF measurements of an X-band accelerating structure for linearizing the longitudinal emittance at SPARC", NIM A 554, (2005), 1-12.
3)   G. Loew and R. Talman, " Elementary principles of Linear Accelerators ", SLAC-PUB-3221, Sept. 1983.
4)   J. W. Wang, " RF properties of periodic accelerating structures for linear colliders ", SLAC-339, July 1989.

5) V.A. Dolgashev et al., "Status of X-band SW Structures studies at SLAC", SLAC-PUB 10124, Aug. 2003.
6) D. Alesini et al., ibid 2.
7) J. Wang J. and T. Higo, " Accelerator Structure Development for NLC/GLC ", SLAC-PUB 10370, Febr. 2004.
8) J. W. Wang et al., " Recent progress in R&D of Advanced Room Temperature Accelerator Structures ", Proceedings of the Linac2002 Conference.
9) G. A. Loew et al., The Stanford Two Mile Accelerator, 1968 W. A. Benjiamin, Inc, pp. 146-148.
10) R. H. Helm, "A Note on the Coupler Asymmetries in Long Linear Accelerators ", Rept. No M-167, SLAC, Stanford University, Stanford, California, Oct. 1963.
11) H. Deruyter et al., " Symmetrical Double Input Coupler Development ", SLAC-PUB-5887, Aug. 1992.
12) K. Watanabe et al., "Double-Feed Coupler for the Linear Collider", Linac1996 Conference,
13) C. Suzuki et al., " Input Coupler Design for C-band Accelerator Structure ", KEK Preprint 97-49, June 1997.
14) www.ansoft.com
15) www.ansys.com